European Journal of Nuclear Medicine and Molecular Imaging (2021) 48:1915–1931
https://doi.org/10.1007/s00259-020-05132-y

ORIGINAL ARTICLE

Biodistribution, pharmacokinetics, dosimetry of [^{68}Ga]Ga-DOTA.SA.FAPi, and the head-to-head comparison with [^{18}F]F-FDG PET/CT in patients with various cancers

Sanjana Ballal[1] · Madhav Prasad Yadav[1] · Euy Sung Moon[2] · Vasko S. Kramer[3] · Frank Roesch[2] · Samta Kumari[1] · Madhavi Tripathi[1] · Sreedharan Thankarajan ArunRaj[1] · Sulochana Sarswat[1] · Chandrasekhar Bal[1]

Received: 22 September 2020 / Accepted: 18 November 2020 / Published online: 26 November 2020

Abstract

Purpose [^{68}Ga]Ga-labeled fibroblast activation protein inhibitors ([^{68}Ga]Ga-FAPi) have shown promising preclinical and clinical results in PET imaging. The present study aimed to evaluate the biodistribution, pharmacokinetics, and dosimetry of [^{68}Ga]Ga-DOTA.SA.FAPi, another modified FAPi tracer, and performed a head-to-head comparison with [^{18}F]F-FDG PET/CT scans in patients with various cancers.

Methods In this prospective study, patients underwent both [^{18}F]F-FDG and [^{68}Ga]Ga-DOTA.SA.FAPi PET/CT scans 60 min post-injection (p.i.). Dosimetry studies were conducted in three patients using [^{68}Ga]Ga-DOTA.SA.FAPi serial time-point imaging. The absorbed dose was calculated using OLINDA/EXM 2.2 software. Quantification of the uptake of the tracers was assessed using standardized uptake values corrected for lean body mass (SUL).

Results Fifty-four patients (mean age; 48.4 years) with 14 types of cancers involving 37% breast, 24% lung, 7.4% head and neck (H&N), and remaining 31.6% patients with other histologies were evaluated prospectively. Physiological uptake of [^{68}Ga]Ga-DOTA.SA.FAPi was observed in the liver, kidneys, pancreas, heart contents, and to a lesser extent in the lacrimals, oral mucosa, salivary glands, and thyroid glands. Uptake in the target lesions on [^{68}Ga]Ga-DOTA.SA.FAPi scan was initiated at 10 min, and no additional lesions were detected in the delayed acquisition time points. The pancreas was the organ with the highest absorbed dose (5.46E-02 mSv/MBq). While the patient-based comparison between the radiotracers revealed complete concordance in the detection of primary, pleural thickening, bone and liver metastases, and second primary malignancy, discordant findings were observed in the detection of lymph node (7.5%), lung nodules (5.6%), and brain metastases (2%). According to the site of primary disease, patients with H&N cancers demonstrated the highest SULpeak and average (avg) values on [^{68}Ga]Ga-DOTA.SA-FAPi which was similar to the values of [^{18}F]F-FDG [(SULpeak: 15.4 vs. 14.2; P-0.680) (SULavg: 8.3 vs. 7.9; P-0.783)]. The lowest uptake was observed in lung cancers with both the radiotracers [(SULpeak: 5.8 vs. 7.4; P-0.238) (SULavg: 4.9 vs. 5.3; P-0.313)]. A significantly higher SULpeak and SULavg for brain metastases to normal brain parenchyma ratios were observed on [^{68}Ga]Ga-DOTA.SA.FAPi in contrast to the [^{18}F]F-FDG values {SULpeak: median: 59.3 (IQR: 33.5–130.8) versus 1.5 (1–2.3); P-0.028}. Except for brain metastases, comparable SULpeak and average values were noted between the radiotracers in all other regions of metastases with no significant difference.

Conclusion [^{68}Ga]Ga-DOTA.SA.FAPi is a promising alternative among the FAPI class of molecules and performed well as compared to standard-of-care radiotracer [^{18}F]F-FDG in the diagnosis of various cancers.

Keywords [^{68}Ga]Ga-DOTA.SA.FAPi PET/CT · Biodistribution · Dosimetry · Pharmacokinetics · Diagnosis

Sanjana Ballal and Madhav Prasad Yadav contributed equally to this work.

This article is part of the Topical Collection on Radiopharmacy

✉ Chandrasekhar Bal
csbal@hotmail.com

[1] Department of Nuclear Medicine, AIIMS, Ansari Nagar, New Delhi PIN: 110029, India

[2] Department of Chemistry, Johannes Gutenberg University, Mainz, Germany

[3] PositronPharma SA, Santiago, Chile

Introduction

To date, [^{18}F]F-FDG PET/CT is the standard-of-care imaging modality in diagnosing various cancers and is based on the principle of the Warburg effect [1]. However, FDG has its own limitations such as low specificity, inability to detect small volume tumors, or lack of uptake in certain cancers, namely mucin-secreting epithelial malignancies, lepidic adenocarcinomas, well-differentiated neuroendocrine tumors, and well-differentiated endocrine gland malignancies [2, 3].

Currently, unlike [^{18}F]-FDG, which is a non-specific metabolic tracer, targeted molecular imaging is experiencing a paradigm shift towards more specific radiotracer imaging. This receptor-specific targeted approach enables the practice of theranostics and likely to achieve the "hallowed goal" of precision oncology. Imaging the tumor microenvironment beyond the glucose or amino acid or fatty acid metabolism is a new norm for understanding the in vivo tumor biology and probably, translating it to clinical oncology practice.

An in-depth understanding of the tumor microenvironment [4] leads to a new player, namely cancer-associated fibroblasts (CAFs). These CAFs are involved in producing growth factors that promote tumor growth, upregulate angiogenesis, mobilize pro-tumorigenic cells, and promote immunosuppression and invasion. Fibroblast activation protein (FAP) is a growth factor that is selectively overexpressed by CAFs and pericytes rather than the tumor cells in more than 90% of the human epithelial malignancies [5]. FAPα is a type II transmembrane glycoprotein that belongs to the superfamily of serine protease, consisting of a primary chain of 760 amino acids with a small intracellular component or a short cytoplasmic tail (6 amino acids), a transmembrane component (19 amino acids), and a large extracellular component [6]. The monomeric form of FAPα is inactive and is activated by dimerization, either homodimer FAPα/FAPα or heterodimer FAPα/FAPβ. This membrane-bound protein is one of the crucial components of the extracellular matrix (ECM) and modulates or remodels the tumor microenvironment.

Fibroblast activating protein inhibitor (FAPi) is a class of biologic probes just at the verge of exploration. The enzymatic activity of FAP provides a therapeutic target in a variety of human malignancies. Therefore, it is an important development for selecting FAP inhibitors (FAPi) in targeting FAP overexpression by CAFs [7].

Based on the concept of a quinoline-based FAP-specific inhibitor (4-quinolinoyl)glycyl-2-cyano-4,4-difluoropyrrolidine, referred to as UAMC1110, [8], currently, a new class of molecules such as FAPI-02 [9, 10], FAPI-04 [9, 10], FAPI-46 [11], and other inhibitory-ligands are designed, synthesized, and evaluated both preclinically and clinically. These imaging probes are highly promising molecular targets when labeled with gallium-68 [9–12] because the biological half-life of these probes is suitably matched with the physical half-life of gallium-68. However, for therapeutic applications, whether with Lu-177 or Ac-225, the biological half-life of these abovementioned probes is not suitable. The search is ongoing to have a molecule that will be true both for imaging and therapy.

Recently, another novel FAP inhibitor (Fig. 1), with further improvised structural changes based on the introduction of squaric acid (SA) motif, namely ^{68}Ga-labeled DOTA.SA.FAPi, has been introduced and evaluated in animal models [13].

The simple coupling chemistry of squaric acid motif increases the biological half-file of the probe which has been shown by our group in an animal study and in theranostic applications [13]. The preclinical data on [^{68}Ga]Ga-DOTA.SA.FAPI and [^{177}Lu]Lu-DOTA.SA.FAPi has been studied in an HT-29 human colorectal cancer xenograft mouse model and reveals encouraging results with high target-to-background ratios (TBR), longer biological half-life, and improved pharmacokinetic properties have been reported. The in vitro binding affinities, excellent in vivo and ex vivo data, are already published [13].

Additionally, DOTA.SA.FAPi demonstrates higher tumor-to-background ratios, and the macrocyclic bifunctional DOTA chelator facilitates radiolabelling with both gallium-68 and lutetium-177/yttrium-90/bismuth-213/actinium-225 which makes the DOTA.SA.FAPi molecule promising and applicable to both imaging and therapy. As a proof-of-principal, our group has applied a theranostic concept of [^{68}Ga]Ga-guided [^{177}Lu]Lu-DOTA.SA.FAPi therapy in an advanced-stage breast cancer patient who was refractory all lines of treatment. The patient experienced immediate relief in pain and improvement in the quality of life. This radio-ligand therapy concept is adding a new milestone in precision oncology. However, the findings are preliminary, and the detailed pharmacokinetics and dosimetry data are evolving [14].

To the best of our knowledge, there is no large-scale published human data on the biodistribution and pharmacokinetics of [^{68}Ga]Ga-DOTA.SA.FAPi. Hence, in this collaborative study, we have attempted to assess the biodistribution, pharmacokinetics, dosimetry, and the diagnostic value of [^{68}Ga]Ga-DOTA.SA.FAPi PET/CT and head-to-head compared with the standard-of-care imaging agent, namely the [^{18}F]F-FDG PET/CT in patients having various cancers.

Methodology

Patient recruitment

This prospective study was approved by the Ethics Committee of All India Institute of Medical Sciences (IECPG-22/2020) and was conducted between January 2020 and September 2020.

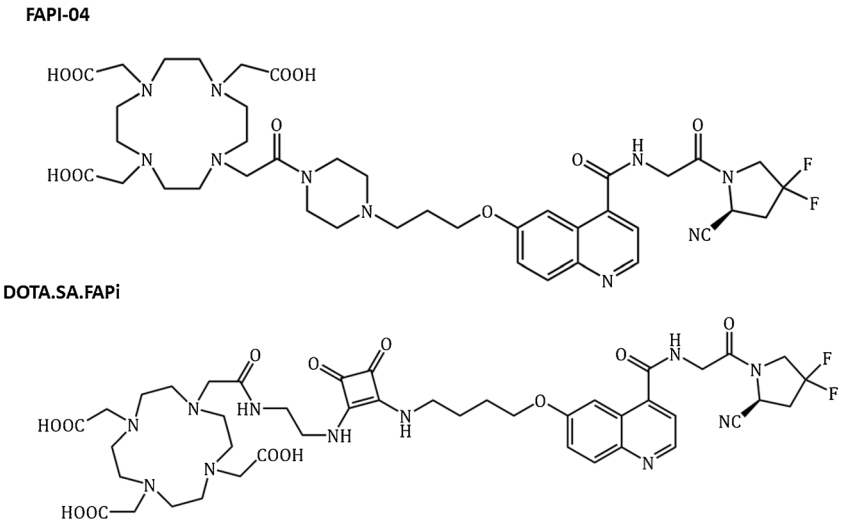

Fig. 1 Molecular structure of FAPI-04 and DOTA.SA.FAPi

Patient selection

The patients were scrutinized using the following eligibility criteria: age > 18 years, histologically confirmed cases of any carcinoma or unknown primary with histological confirmation after PET/CT scans, patients referred to the Nuclear Medicine Department for both [^{18}F]F-FDG and [^{68}Ga]Ga-DOTA.SA.FAPi PET/CT scans and were willing to give written informed consent to participate in this study were included. Exclusion criteria involved patients who denied to undergo [^{68}Ga]Ga-DOTA.SA.FAPi PET/CT imaging, pregnant, and lactating females. Based on the above criteria, 54 patients were included in this study.

Synthesis of [^{68}Ga]Ga-DOTA.SA.FAPi

The DOTA.SA.FAPi molecule was synthesized by Moon et al. [13] under the supervision of Prof. Dr. F. Roesch from the Department of Chemistry, Johannes Gutenberg University of Mainz, Germany, and procured as a part of a collaborative project with Prof. Dr. C. S. Bal, AIIMS, New Delhi, India. The eluted $^{68}GaCl_3$ solution (~ 925 MBq) was added to the reaction vial containing DOTA.SA.FAPi and ammonium acetate and heated at 95 °C for 20 min. The radiolabelled product was eluted through a Sepak C18 cartridge with 50% ethanol followed by 10 ml normal saline. Quality control of the labeled product was performed by high-performance liquid chromatography (radio HPLC) and radiochemical purity of > 94% was accepted for patient injection.

Image acquisition and analysis

All the scans were acquired on a dedicated GE Discovery 710* 128 Slice PET/CT Scanner, with a 40-mm detector at a 0.35-s rotation speed and a 128 slice CT scanner. The images were corrected for random and scatter counts, decay correction, and dead time correction. The PET images were reconstructed with iterative reconstruction using ordered subset expectation maximization algorithm (OSEM) (21 subsets 3 iterations). The images were processed and analyzed with a dedicated commercially available workstation (GE Xeleris).

Image acquisition and analysis for dosimetry

Acquisition protocol

Three patients took part in the dosimetry study. As a prerequisite for imaging, the patient was instructed to void before the [^{68}Ga]Ga-DOTA.SA.FAPi injection. Following the administration of [^{68}Ga]Ga-DOTA.SA.FAPi (mean injected activity: 174 MBq), serial whole-body PET studies were acquired at 0.16, 1, 2, and 3 h post-injection (p.i.). For acquisition, the patient was positioned in a supine position. The acquisition protocol constituted an initial scout image to define the field of view of the acquisition required, followed by a CT scan, and PET acquired at 2 min per bed. A total of two CT scans were acquired for 4 PET image acquisitions. The first CT involved a diagnostic dose CT with 300–350 mAs, 120 kVp, slice thickness 5 mm, and pitch 1. The second CT scan was used only for attenuation correction purposes, which included a low-dose CT protocol of 180 mAs, 80 kVp, 5-mm slice thickness, and pitch 1.

Image analysis

Source organs for analysis included pancreas, kidneys, liver, spleen, heart contents, L2–L4 lumbar vertebrae for red marrow dosimetry, and urinary bladder and its contents. To analyze the absorbed dose, the first step involved the region of interest (ROI) analysis of the above organs. The ROIs for the above organs were drawn on the initial [^{68}Ga]Ga-

DOTA.SA.FAPi PET/CT scan (0.16 h) and was appended/cloned to the consecutive sequential time points.

Three-dimensional (3D) ROIs, rectangular, elliptical, or freehand ROIs were chosen according to the shape of the organ. For organs like the liver and spleen, to prevent to spill-in of activity from the kidneys and other adjacent organs, a two-dimensional ROI was drawn on one slice and stacked to all the slice base on the CT anatomy to deduce the 3D volume. The activity concentration in all the organs was assumed uniform and hence was derived in the form of Bq/cm^3. The activity per centimeter cube was multiplied by the total mass of the corresponding organ. The mass of various source organs was adopted from the anthropomorphic phantom data reported in the annals of ICRP 89 [15].

Calculation of percentage of injected activity, residence times, and the mean absorbed dose

The ratio of mean activity in a source organ to the injected activity multiplied by 100 was defined as the percentage of injected activity (%IA). OLINDA/EXM 2.2 dosimetric software was used to calculate the residence times/number of disintegrations of each source organ. The %IA at time points 0.16, 1, 2, and 3 h for each source organ was entered in the kinetic input model of OLINDA/EXM 1.0, and the mono- or bi-exponential curve fitting parameters were applied to derive the best curve fit for the residence time of activity in the source organ. As the blood sampling method was not a feasible option in the heavily pre-treated chemotherapy patients, red bone marrow dosimetry was done by image-based 3D volumetric analysis of L2–L4 vertebrae, which is considered to constitute 6.7% of the total bone marrow [16].

The patient was instructed to urinate just before the injection of [^{68}Ga]Ga-DOTA.SA.FAPi and advised not to void during the serial dosimetric acquisition of PET/CT images. It was to prevent any biological mode of excretion of tracer from the body and to assume only physical decay of activity.

Once all the organ residence times were derived from the kinetic input model, they were entered in the adult female model data that derived the absorbed doses to all the organs, including the whole-body effective dose, and generated in mSv/MBq and rem/mCi. The time-activity graphs of various organs were generated using GraphPad Prism software.

Image acquisition and analysis for [^{18}F]F-FDG and [^{68}Ga]Ga-DOTA.SA.FAPi PET/CT qualitative and quantitative comparison

Fifty-four patients underwent [^{18}F]F-FDG and [^{68}Ga]Ga-DOTA.SA.FAPi PET/CT for biodistribution and a head-to-head intra-individual comparison between the traces.

Acquisition protocol

While for [^{18}F]-FDG PET/CT, patients were advised to fast for at least 4–6 h prior to injection, no such preparation was required for a [^{68}Ga]Ga-DOTA.SA.FAPi scan. The mean injected activities were 271 MBq (range: 185 to 370 MBq) and 144.3 MBq (range: 59.2 to 296 MBq) for [^{18}F]F-FDG and [^{68}Ga]Ga-DOTA.SA.FAPi radiotracers, respectively. Patients underwent [^{68}Ga]Ga-DOTA.SA.FAPi PET/CT scans within a 1-week interval of [^{18}F]F-FDG PET/CT. The same parameters for acquisition were followed as stated above in the dosimetry acquisition section but were acquired only approximately at 1 h p.i. using diagnostic CT parameters. Spot views were acquired for brain metastases patients with a slice thickness of 3 mm on CT at 120 kVp, 100 mAs, and a pitch of 0.6.

Image analysis

[^{18}F]F-FDG and [^{68}Ga]Ga-DOTA.SA.FAPi PET/CT scans were loaded simultaneously and co-registered using carina as an anatomical landmark registration technique. Scan interpretations were conducted by 2 experienced nuclear medicine physicians. Any disagreement in the reports was reviewed by a third observer.

Qualitative analysis

Qualitative interpretations of both the scans were made to compare the visual expression and the concordance of the uptake between the tracers. The uptake in both the tracers was finally matched to the corresponding lesion morphology on CT. Any discordance was reconfirmed either by histopathological correlation or by MR imaging. Disease foci were divided into four anatomical sites: local disease (primary/residual tumor), nodal metastases, distant metastases (pulmonary, skeletal, liver, brain, etc.), and other metastatic or malignant sites not known earlier (new site).

Quantitative analysis

For the quantitative comparison, ROIs were drawn according to the PET Response Criteria in Solid Tumors (PERCIST 1.0) [17]. The ROI for various organs and lesions was drawn on [^{18}F]F-FDG PET/CT scan and cloned on to the [^{68}Ga]Ga-DOTA.SA.FAPi PET/CT scan. The ROIs were presented as standardized uptake value (SUV) corrected for lean body mass, SULpeak, and SULavg to quantitatively compare the uptake in the normal organs and cancer involved regions.

To calculate the SUL in normal organs, ROIs of 1.2 cm were drawn in order to produce a 1 cm^3 volume in the mediastinal blood pool, pancreas, left psoas major muscle, myocardium, spleen, salivary glands, thyroid, duodenum, normal parenchyma of the brain, and spherical ROIs of 3-cm diameter

Table 1 Detailed demographics and extent of disease of patients

Patient no	Age/ gender	Type of cancer	Extent of cancer
1	48/M	Olfactory neuroblastoma	Primary
2	25/M	Colon cancer	Primary, lymph node
3	48/F	Right breast cancer, ER +, PR +, Her2neu−	Liver, lung, brain
4	72/M	Pleural mesothelioma	Primary, lymph node, pleural thickening
5	40/F	Adenoid cystic carcinoma of the liver	Primary, lymph node
6	65/M	Non-small cell lung cancer	Primary, lymph node
7	32/F	Right breast cancer, ER+, PR+, Her2neu−	Lymph node, liver, skeletal
8	66/F	Breast cancer, triple negative	Lymph node, lung,
9	45/M	Left buccal mucosa squamous cell carcinoma	Primary, lymph node
10	45/F	Colon cancer	Primary, lymph node, lung
11	63/F	Rectal cancer	Krukenberg metastases
12	48/F	Right breast cancer, ER+, PR+, Her2neu−	Liver, lung, brain, pleural thickening, stomach second primary
13	41/F	Left breast cancer, TNBC	Liver, skeletal, Krukenberg metastases
14	37/F	Gallbladder cancer	Primary
15	*50/F*	*Right breast cancer, ER+, PR+, Her2neu−*	*Primary, Lung, skeletal*
16	56/F	Bilateral breast cancer, ER−, PR−, Her2neu+	Lymph node, brain
17	54/F	Left breast cancer, ER+, PR+, Her2neu−	Lymph node, skeletal, brain
18	30/F	Bilateral breast cancer, ER−, PR−, Her2neu+	Primary, lymph nodes, lung, skeletal, liver, brain
19	45/F	Right breast cancer, ER−, PR−, Her2neu+	Primary, lymph nodes, lung, liver
20	43/F	Non-small cell lung cancer	Primary, lymph nodes, lung, pleural thickening
21	45/F	Breast cancer, ER−, PR−, Her2neu+, invasive ductal carcinoma	Primary, lymph node, lung, liver
22	*38/F*	*Left breast cancer, TNBC, invasive ductal carcinoma*	*Primary, lymph node, lung*
23	50/F	Right breast cancer, TNBC	Lung, skeletal
24	62/F	Breast cancer, ER+, PR+ Her2neu−	Primary, lymph node, lung, pleural thickening
25	54/M	Right lung cancer, NSCLC (adenocarcinoma)	Primary, lymph node, lung
26	37/F	Left breast cancer, TNBC	Primary, lymph node, liver, muscle
27	36/M	Lung cancer adenocarcinoma	Primary, lymph node, pleural thickening, brain
28	15/F	Non-Hodgkin's lymphoma B cell of the ovary	Skeletal metastases
29	56/M	Unknown primary Post-FAPi and FDG PET scans followed by Bx: (squamous cell carcinoma of the neck)	Primary, lymph node, brain, muscle
30	67/F	Multiple myeloma	Primary, lymph node
31	46/F	Mesenteric carcinoid	Primary, lymph nodes, lung, liver, adrenals
32	61/F	Right lung cancer, NSCLC (adenocarcinoma)	Primary, lymph node
33	41/F	B/L ovarian carcinoma	Primary, lymph nodes, serosal and omental deposits
34	*47/F*	*Non-small cell lung cancer (squamous cell carcinoma)*	*Primary, lymph nodes, lung*
35	37/M	Hodgkin's lymphoma	Lymph node
36	54/F	B/L breast cancer, ER−, PR−, Her2neu+	Lymph node, lung, skeletal, liver, brain
37	10/M	Glioblastoma multiforme	Primary
38	48/M	Olfactory neurofibroblastoma	Primary
39	48/F	Adenocarcinoma lung	Primary, lymph node, lung, pleural thickening, liver, brain
40	54/F	Unknown primary Post-FAPi and FDG PET scans followed by Bx: (left breast cancer)	Lymph node, liver, lung mass, skeletal
41	57/F	Ovarian cancer	Primary, lymph node
42	69/M	Right lung cancer NSCLC (SCC)	Primary, lymph node, lung
43	52/M	Right lung cancer NSCLC (adenocarcinoma)	Primary, lymph node, lung
44	45/M	Multiple myeloma	Lymph node, lung, liver, skeletal, brain, B/L adrenals, omental nodules

Table 1 (continued)

Patient no	Age/ gender	Type of cancer	Extent of cancer
45	42/F	Right breast cancer, ER−, PR+, Her2neu+	Brain metastases
46	33/F	Right breast cancer, TNBC	Lymph node, lung, pleural thickening, skeletal, muscle
47	66/M	Unknown primary Post-FAPi and FDG PET scans followed by Bx: (base of the tongue, squamous cell carcinoma)	Primary, lymph node
48	58/F	Right lung cancer, NSCLC (adenocarcinoma)	Primary, lymph nodes, lung, skeletal, liver, thyroid cartilage, adrenals
49	45/M	Glottic cancer, squamous cell carcinoma	Primary, lymph nodes
50	60/M	Right lung cancer, NSCLC (adenocarcinoma)	Primary, lymph nodes, lung, pleural thickening, lymph node, brain
51	33/F	Right breast cancer	Lymph node, lung, lung mass, liver, skeletal, brain, adrenals
52	56/M	Gall bladder cancer	Primary, lung
53	66/M	Right lung cancer, sarcomatous ca with focal squamous cell differentiation	Primary, lymph node, lung, pleural thickening, skeletal, liver, adrenals
54	60/M	Left lung cancer, NSCLC (modified differentiated SCC)	Primary, lymph node, lung, pleural thickening

The italics represent the patients on whom the dosimetry was performed (not significant)

M, male; *F*, female; *ER*, estrogen receptor; *PR*, progesterone receptor; *Her2neu*, human epidermal growth factor receptor 2; *TNBC*, triple-negative breast cancer; *NSCLC*, non-small cell lung cancer; *SCC*, squamous cell carcinoma

were drawn in the right lobe of the liver. To compare the uptake in the lesions, a 3D auto-contour ROI at a 40% threshold of SULpeak was carefully drawn around the site of [^{18}F]F-FDG/[^{68}Ga]Ga-DOTA.SA.FAPi expressing lesions. TBRs were also calculated according to the site of the lesion and with various combinations of backgrounds such as liver, spleen, pancreas, blood pool, and muscle uptake.

Statistical analysis

The data were analyzed for normality using the D'Agostino-Pearson test. Mean, median, standard deviation (SD), range, and interquartile range (IQR) were calculated for all continuous variables based on the distribution of data. The analysis was done on an intra-individual basis. The concordance and discordance were presented in the form of a percentage. Weighted kappa statistics were used to assess the level of agreement between the two observers in assessing the [^{68}Ga]Ga-DOTA.SA.FAPi PET/CT scan. It was calculated as follows: $(P0 - Pe)/(1\text{-}Pe)$, where $P0$ is the observed agreement, Pe is the agreement by chance, and $(1\text{-}Pe)$ is the proportion of the cases for which would predict disagreement between the raters. Kappa values < 0.4 meant poor agreement, values between 0.4 and 0.75 indicate fair to good agreement, and values of 0.75 and higher represent excellent agreement [18]. Paired Student's *t* test or Wilcoxon signed-rank test was used to compare the organ and lesion uptake values between and [^{18}F]F-FDG and [^{68}Ga]Ga-DOTA.SA.FAPi PET/CT scans. P value < 0.05 was considered statistically significant. Statistical analysis was performed using MedCalc statistical software.

Results

Patients

The detailed clinical history and extent of cancer spread of 54 patients (mean age; 48.4 ± 12.4, 19–72 years) are depicted in Table 1.

Across the patients referred, three had unknown primaries that were diagnosed on both [^{18}F]F-FDG and [^{68}Ga]Ga-DOTA.SA.FAPi PET/CT and later confirmed on histopathology as infiltrating duct carcinoma of the breast, squamous cell carcinoma (SCC) of the base of the tongue, and SCC of the neck, respectively.

Among the various primary malignancies, breast cancer (37%, 20/54) followed by lung cancer (24%, 13/54) constituted the major sub-categories of the patients included (Table 1). The [^{68}Ga]Ga-DOTA.SA.FAPi injection was well tolerated, and no adverse events were observed throughout the scanning procedure.

Biodistribution and pharmacokinetics of [^{68}Ga]Ga-DOTA.SA.FAPi

The dosimetry was conducted in 3 female patients (2 breast cancer and 1 lung cancer patient) with a mean age of 45 ± 6 years (38–50). The physiological biodistribution of [^{68}Ga]Ga-DOTA.SA.FAPi involved the pancreas, liver, heart contents, spleen, kidneys, urinary bladder, and to a lesser extent, in the lacrimals, oral mucosa, salivary glands, and thyroid glands.

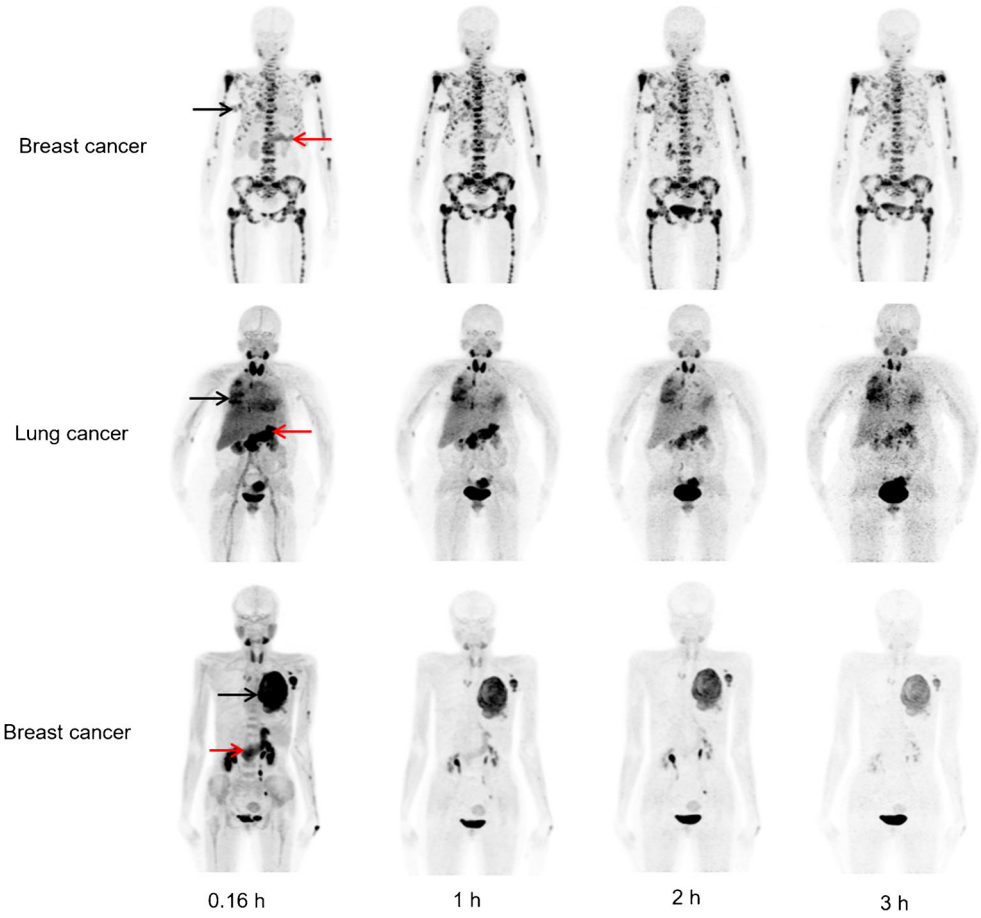

Fig. 2 Biodistribution of [^{68}Ga]Ga-DOTA.SA.FAPi at serial time points in breast and lung cancer patients with primary lesions (black arrow) and metastases involving lymph nodes, liver, and bone. There is a rapid accumulation of tracer seen in the 10-min image with retention until 3-h images. Radiotracer accumulation is also seen in the pancreas (red arrows), salivary glands. Steady clearance of blood pool activity with visualization of kidneys, ureter, and urinary bladder noted in serial images

Visual analysis revealed the pancreas as the organ of the highest uptake. Figure 2 demonstrates serial images that depict the normal biodistribution and expression of [^{68}Ga]Ga-DOTA.SA.FAPi in a patient with carcinoma of breast showing extensive metastases to various organs (Fig. 2).

Uptake in the normal organs, primary tumor, and the metastases was detectable as early as 10 min p.i. and remained visible up to 3 h of imaging (Fig. 2). All the organs showed an exponential decrease in the activity which was fitted using either mono-exponential or bi-exponential curve fitting. The washout of the radiotracer from the bone marrow was rapid, with a decrease in the %IA to > 50% of its initial value at 60 min p.i. (Fig. 3a). Similarly, the washout in the remaining organs with normal physiological uptake (Fig. 3a) and the remainder of the body (Fig. 3b) was rapid all throughout the time span of 3 h.

Interestingly, the uptake in all the lesions initially showed a decrease from the 10 min to the 1 h time point but remained relatively stable with only a mild decrease throughout up to 3 h p.i. (Fig. 4).

In contrast to a subtle decrease in the SULavg values in the lesions, there is a rapid washout of the radiotracer from the normal organs such as the liver, pancreas, blood pool, left psoas muscle (Fig. 4 and Table 2). Accordingly, the maximum target-to-background ratio (TBR) in the lesions steadily increased over time, even up to 3 h of the scan with a steady and significant decrease in the background activity. The highest TBR uptake was observed using the lesion-to-psoas muscle ratio.

Among the categories of lesions, the highest lesion-to-psoas muscle ratio was observed in skeletal metastases wherein the TBR was 9.33 at 10 min and 7.6 at 3 h with an 18% drop from its initial value. The next highest TBR was found in the liver, followed by the blood pool, and the pancreas decreasing order (Table 2).

A detailed comparison of SULavg uptake values in various types of cancer lesions at 10 min and 3 h post-[^{68}Ga]Ga-DOTA.SA.FAPi injection revealed a decline in the radiotracer uptake by 7.9% (SULavg: 6.95 to 6.6), 6.8% (SULavg: 5.89 to 5.42), 22.6% (SULavg: 7.62 to 5.9), 44.3% (SULavg: 9.7 to 5.4), and 14.7% (SULavg: 5.5 to 4.7) in the primary tumor, LN metastases, liver metastases, skeletal metastases, and brain metastases, respectively (Fig. 4). Another interesting finding was that the number of lesions detected in the 1st time point (i.e., 0.16 h p.i. scan) did not differ from the other time-point scans.

The mean fraction of activity excreted into the urinary bladder was double in the first 60 min. Figure 3c

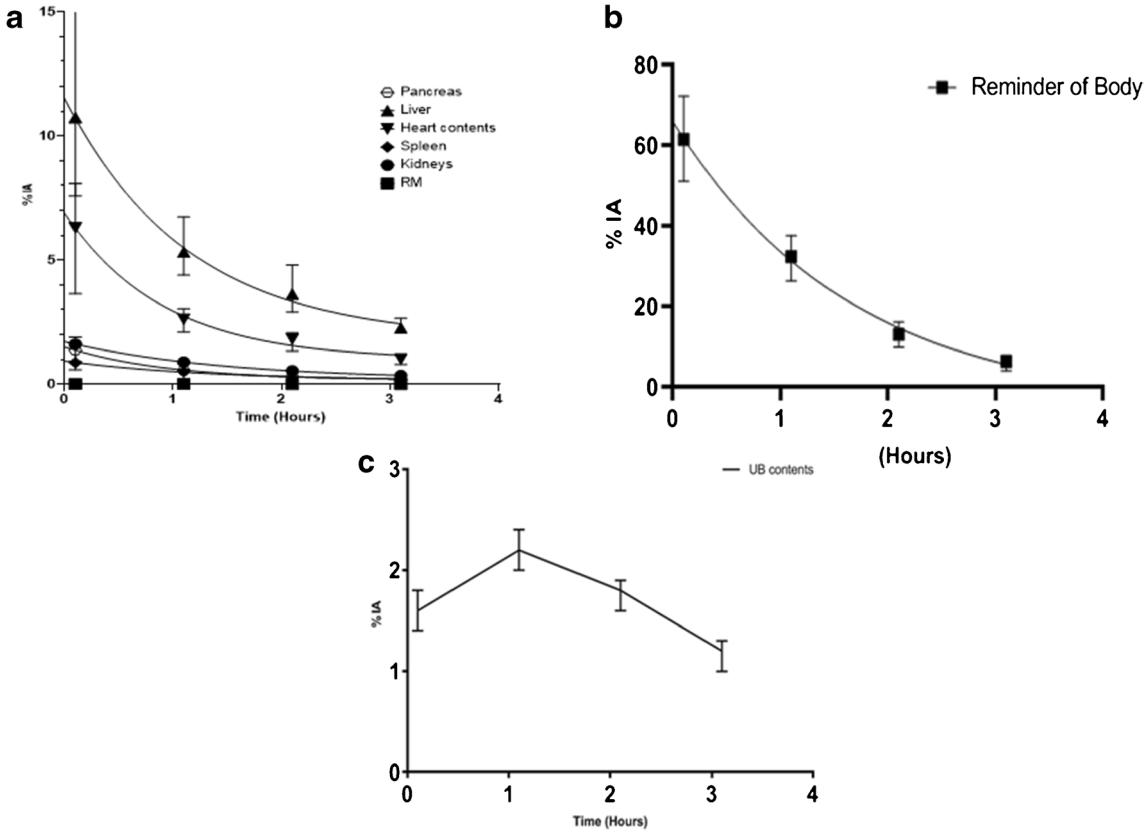

Fig. 3 Percentage of injected activity (IA) of [^{68}Ga]Ga-DOTA.SA.FAPi in organs with normal physiological uptake (**a**), %IA in the remainder of the body (**b**), and %IA in the urinary bladder without voiding (no biological excretion) (**c**)

depicts the %IA in the urinary bladder contents without voiding between the scans derived from curve fitting. Considering that no biological excretion took place during the temporal acquisition period, the %IA curve of the urinary bladder demonstrated an initial increase in the activity followed by a decreasing trend reflecting the collection and the physical decay of activity in the urinary bladder.

Dosimetry

The mean residence times in source organs, such as the heart contents, kidneys, liver, pancreas, red marrow, spleen, urinary bladder contents, and the remainder of the body were 4.20E-02, 1.41E-02, 1.01E-01, 9.76E-03, 8.53E-04, 7.93E-03, 3.03E-02, and, 4.86E-01 MBq-h/MBq, respectively. Table 3 details the dosimetry estimate of absorbed dose in each organ,

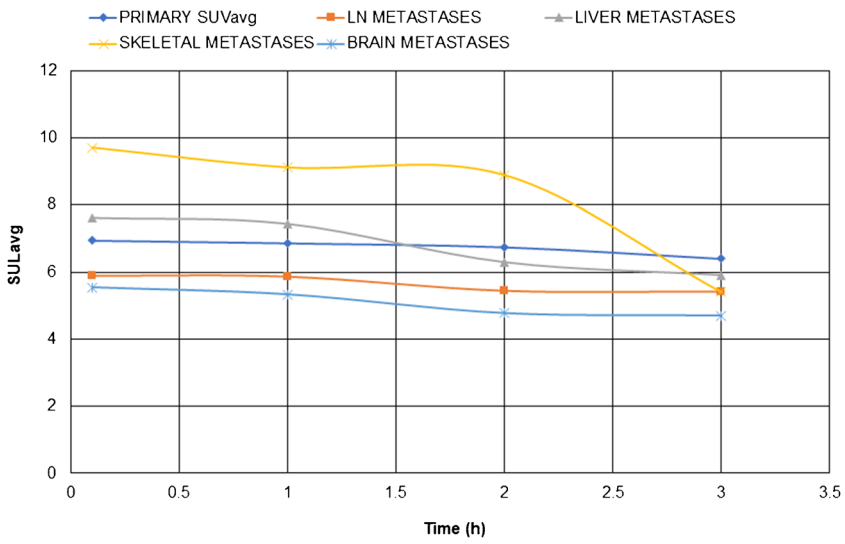

Fig. 4 Mean standardized uptake value patterns of [^{68}Ga]Ga-DOTA.SA.FAPi in lesions in 3 patients at various time points. The highest SULavg values observed were skeletal metastases

Table 2 Target-to-background ratios of [^{68}Ga]Ga-DOTA.SA.FAPi at various time-points post-injection in three patients

Primary tumor				
Time point (h)	Primary tumor/liver Bkg	Primary tumor/psoas muscle Bkg	Primary tumor/pancreas Bkg	Primary tumor/blood pool Bkg
0.16	2.27	6.68	1.01	1.12
1	2.28	6.80	1.32	1.32
2	3.05	7.84	1.50	2.63
3	3.15	9.01	2.46	3.55
Lymph node metastases				
Time point (h)	LN metastases/liver Bkg	LN metastases/psoas muscle Bkg	LN metastases/pancreas Bkg	LN metastases/blood pool Bkg
0.16	1.93	5.66	0.85	0.95
1	1.94	5.80	1.12	1.12
2	2.46	6.32	1.20	2.12
3	2.66	7.63	2.08	3.01
Liver metastases				
Time point (h)	Liver metastases/liver Bkg	Liver metastases/Psoas muscle Bkg	Liver metastases/pancreas Bkg	Liver metastases/blood pool Bkg
0.16	2.49	7.32	1.11	1.22
1	2.47	7.36	1.43	1.43
2	2.84	7.31	1.39	2.45
3	2.90	8.30	2.26	3.27
Skeletal metastases				
Time point (h)	Skeletal metastases/liver Bkg	Skeletal metastases/psoas muscle Bkg	Skeletal metastases/pancreas Bkg	Skeletal metastases/blood pool Bkg
0.16	3.18	9.33	1.41	1.56
1	3.02	9.02	1.75	1.75
2	4.02	10.33	1.97	3.47
3	2.66	7.60	2.07	3
Brain metastases				
Time point (h)	Brain metastases/liver Bkg	Brain metastases/psoas muscle Bkg	Brain metastases/pancreas Bkg	Brain metastases metastases/blood pool Bkg
0.16	1.81	5.32	0.80	0.89
1	1.77	5.27	1.02	1.02
2	2.15	5.54	1.06	1.86
3	2.31	6.61	1.80	2.61

Bkg, background; *LN*, lymph node metastases

Table 3 Absorbed dose estimate of [^{68}Ga]Ga-DOTA.SA.FAPi

Organ	Mean absorbed doses (mSv/MBq)	Mean absorbed doses (rem/mCi)
Adrenals	7.77E-03	2.87E-02
Brain	5.06E-03	1.87E-02
Breast	5.48E-03	2.03E-02
Gallbladder wall	8.37E-03	3.10E-02
LLI wall	6.41E-03	2.37E-02
Small intestine	6.26E-03	2.32E-02
Stomach wall	6.93E-03	2.56E-02
ULI wall	6.65E-03	2.46E-02
Heart wall	3.16E-02	1.17E-01
Kidneys	2.62E-02	9.68E-02
Liver	3.84E-02	1.42E-01
Lungs	6.62E-03	2.45E-02
Muscle	5.79E-03	2.14E-02
Ovaries	6.48E-03	2.40E-02
Pancreas	5.46E-02	2.02E-01
Red marrow	4.80E-03	1.78E-02
Osteogenic cells	8.66E-03	3.20E-02
Skin	4.96E-03	1.83E-02
Spleen	2.68E-02	9.91E-02
Thymus	6.56E-03	2.43E-02
Thyroid	5.34E-03	1.97E-02
Urinary bladder wall	5.21E-02	1.93E-01
Uterus	6.98E-03	2.58E-02
Total body	7.05E-03	2.61E-02
Effective dose equivalent	1.64E-02	6.08E-02
Effective dose	1.11E-02	4.10E-02

LLI, lower large intestine; *ULI*, upper large intestine

effective dose equivalent, and the effective dose. The organ with the highest radiation absorbed dose was the pancreas (5.46E-02 mGy/MBq) followed by the urinary bladder wall (5.21E-02 mGy/MBq), liver (3.84E-02 mGy/MBq), heart wall (3.16E-02 mS/MBq), spleen (2.68E-02 mGy/MBq), and kidneys (2.62E-02 mGy/MBq). The mean effective dose equivalent (EDE) was (1.64E-02 mSv/MBq). The estimated mean effective dose was 0.011 mSv/MBq. The mean effective dose from 185 MBq of [^{68}Ga]Ga-DOTA.SA.FAPI is estimated to be 2 mSv.

Comparison between and [^{18}F]F-FDG and [^{68}Ga]Ga-DOTA-SA-FAPi PET/CT scans

There was a complete inter-observer agreement for all organs with physiological biodistribution on [^{68}Ga]Ga-DOTA.SA.FAPi PET/CT. Similarly, on the [^{68}Ga]Ga-DOTA.SA.FAPi PET/CT scans, for uptake in the lesions situated in the primary, pleural thickening, bone metastases, liver, brain, and second primary malignancies, the degree of inter-observer agreement was 1. Though there was disagreement between the observers in detecting the lymph node and lung metastases, the agreement level was high: 0.82 and 0.87, respectively.

Normal organ uptake comparison

Except for uptake in the pancreas which showed significantly higher uptake of [^{68}Ga]Ga-DOTA.SA.FAPi when compared to [^{18}F]F-FDG, all other organs showed similarities in both tracers' physiological uptake (Fig. 5a and b, Supplementary Table 1). Despite the similarities, a significantly high SULpeak and average uptake values were noted in the pancreas, salivary glands, thyroid, and the psoas muscle on [^{68}Ga]Ga-DOTA.SA.FAPi PET/CT scans in contrast to [^{18}F]F-FDG PET/CT (Fig. 5a and b, Supplementary Table 1). Both the tracers demonstrated low blood pool activity across all the scans. In organs such as spleen, duodenum, vertebrae, and extremities like femur, the quantitative uptake was slightly higher on the [^{18}F]F-FDG PET/CT scans.

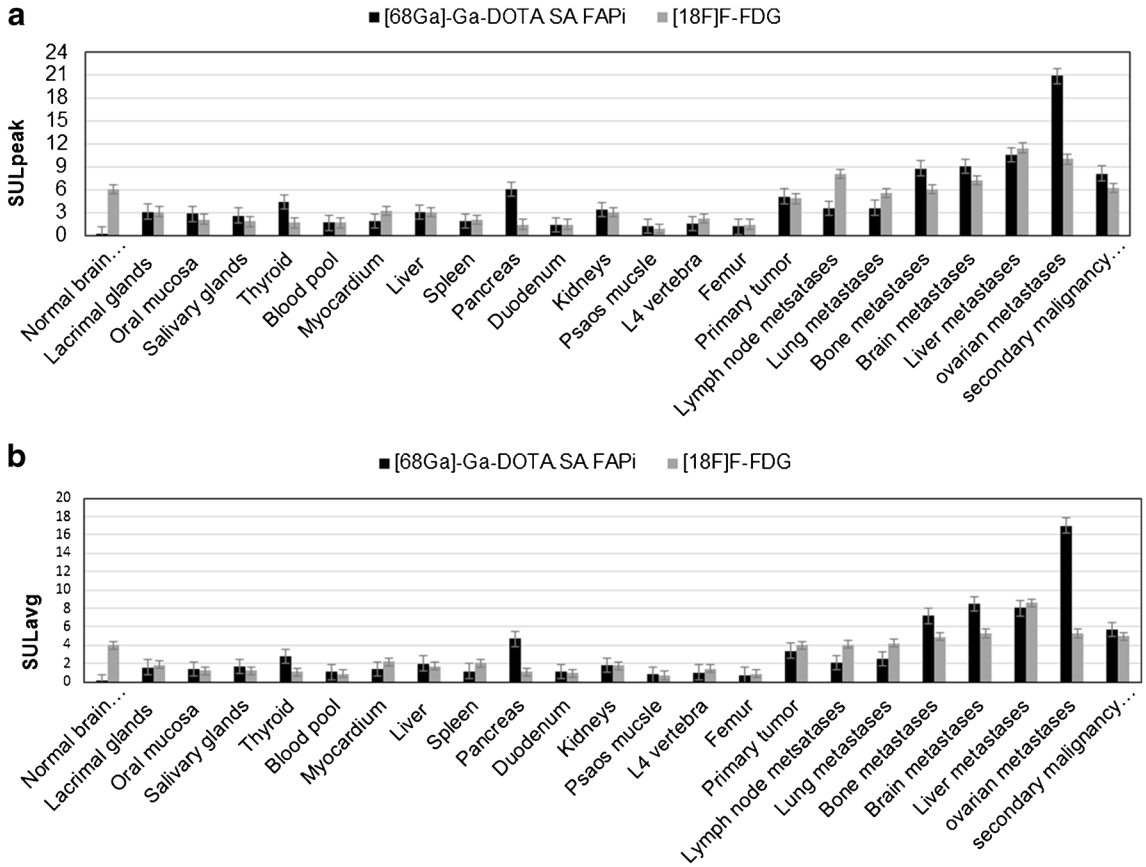

Fig. 5 Comparison of SULpeak (**a**) and the SULavg (**b**) values between [^{18}F]F-FDG and [^{68}Ga]Ga-DOTA.SA.FAPi radiotracers in 20 patients at 1 h after injection

Contrary to the avid uptake of [^{18}F]F-FDG in the normal brain parenchyma, an outstandingly negligible uptake was quantified on [^{68}Ga]Ga-FAPi PET/CT scan aiding a better diagnosis of the brain metastases (Fig. 5a and b, Supplementary Table 1).

Comparison according to the site of malignancy or metastases

Patient-based analysis

A comprehensive comparison of median SULpeak and SULavg values amidst the tracers in various primary disease sites and metastases are detailed in Tables 4 and 5; Supplementary Table 3, respectively.

Primary tumor

Thirty-seven patients were detected with primary residual tumor uptake, and a complete concordance was observed between both tracers. Referring to the intensity of the tracer accumulation in the primary/residual tumor site, the median SUL values were comparable between the tracers {[^{18}F]F-FDG:6.1; (IQR: 3.5–7.4) vs [^{68}Ga]Ga-DOTA.SA.FAPi: 4.4; (IQR: 2.8–8.7), P-0.843} (Table 4). Furthermore, a subcategorical analysis was conducted according to primary cancer, and comparable results were noted between the two tracers (Table 5).

Lymph node

Concordance for detection of lymph node metastases between [^{68}Ga]Ga-DOTA.SA.FAPi and [^{18}F]F-FDG PET/CT scan was 92.5% (50/54). Regarding the intensity of tracer accumulated in the lymph nodes, the SULpeak was higher for [^{18}F]F-FDG PET/CT than the [^{68}Ga]Ga-DOTA.SA.FAPi; however, the difference was not significant [5 (IQR: 1.7–9.6) vs. 3.7 (IQR: 1.9–6.8), P-0.672] (Table 4). Among the 4 patients with discordant LN metastases findings, [^{68}Ga]Ga-DOTA.SA.FAPi scan was false negative in 2 cases, and [^{18}F]F-FDG was false positive in two cases, respectively (Supplementary Table 3) (Figs. 6 and 7).

Lung-related lesions and liver metastases

While 51 (94.4%) patients showed agreement between the detection of lung metastases, [^{68}Ga]Ga-DOTA.SA.FAPi

Table 4 Comparison of SUL values between [^{68}Ga]Ga-DOTA.SA.FAPi and [^{18}F]F-FDG PET/CT in primary tumor and metastases

Region of malignancy/ metastases	SULpeak [^{68}Ga]Ga-DOTA.SA.FAPi PET/CT median (IQR)	SULpeak [^{18}F]F-FDG PET/CT median (IQR)	*P* value	SULavg [^{68}Ga]Ga-DOTA.SA.FAPi PET/CT median (IQR)	SULavg [^{18}F]F-FDG PET/CT median (IQR)	*P* value
Primary	6.1 (3.5–7.4)	4.4 (2.8–8.7)	0.843	5.1 (2.3–5.8)	3.84 (1.4–6.6)	0.843
Lymph node	3.7 (1.9–6.8)	5(1.7–9.6)	0.672	2.5 (1.2–4)	3 (1.1–5.2)	0.946
Skeletal	7.9 (5.4–10.9)	4.5 (3–6.8)	0.125	6 (3.2–8.8)	3.5 (2.2–5.1)	0.225
Lung	5.7 (1.9–9.3)	5.4 (2.2–8.3)	0.375	3.2 (1.1–5.2)	4 (2.2–5.4)	0.215
Liver	10.1 (6.5–12.5)	11.4 (6.1–14.5)	0.875	6.6 (4.2–7.6)	7.6 (4–11)	0.625
Brain	10.1 (5.7–14.9)	7.7 (5.1–9.8)	0.477	8.0 (4.6–13.9)	5.0 (4.2–6.8)	0.489
Pleural thickening	7(2.8–8)	10.7 (4–13.9)	0.386	4.8 (1.8–6.9)	6.5 (2.9–9.1)	0.421
Secondary malignancy in stomach ($N = 1$)	8.12	6.6	-	5.7	5	-
Ovarian metastases ($N = 2$)	20.09	10	< 0.0001	17	5.3	< 0.0001

SULpeak and avg, standardized uptake value corrected for lean body mass; *IQR*, interquartile range

proved superior in three patients, among whom 2 were falsely positive, and 1 was false negative on [^{18}F]F-FDG. A complete concordance was demonstrated in patients with pleural thickening. Similar radiotracer uptake values were noted between the two agents (Tables 4 and 5; Supplementary Table 3). A complete concordance was noticed between the tracers for liver metastases with no significant difference in the uptake values (Tables 4 and 5; Supplementary Table 3).

Skeletal metastases

Both the tracers identified all sites of skeletal metastases in all patients (Supplementary Table 3). Despite the visual resemblance, when quantified, a marginally higher uptake was documented on [^{68}Ga]Ga-DOTA.SA.FAPi scans compared to [^{18}F]F-FDG scans but was not significant {SULpeak: [7.9 (5.4–10.9) vs.4.5 (3–6.8), P-0.125], SULavg [6 (3.2–8.8) vs 3.5(2.2–5.1), P-0.225]} (Table 4).

Brain metastases

Both the tracers identified brain metastatic lesions in 12 patients. Five patients demonstrated multiple brain metastases, but [^{18}F]F-FDG PET/CT failed to identify all the brain lesions in one patient (Fig. 8). On quantification of tracer uptake, a remarkably higher SULpeak and SULavg brain metastases-to-brain normal parenchyma ratios were observed on [^{68}Ga]Ga-DOTA.SA.FAPi in contrast to the [^{18}F]F-FDG values: {SULpeak: [^{68}Ga]Ga-DOTA.SA.FAPi; median: 83.2 (IQR: 34.2–249.3) vs. [^{18}F]F-FDG; 1.5 (1–2.3); P-0.028} and {SULavg: [^{68}Ga]Ga-DOTA.SA.FAPi; median: 59.3 (IQR: 33.5–130.8) versus [^{18}F]F-FDG; 1.2 (1–2.3); P-0.029}. (Fig. 8).

Metastases to other sites

In two patients with breast cancer as the primary, Krukenberg metastases were detected, but an outstandingly high uptake was noted on [^{68}Ga]Ga-DOTA.SA.FAPi PET/CT scans

Table 5 Comparison of SUL values according to the site of the primary tumor

Site of Primary cancer	SULpeak [^{68}Ga]Ga-DOTA.SA.FAPi PET/CT (mean ± SD, range)	SULpeak [^{18}F]F-FDG PET/CT (mean ± SD, range)	*P* value	SULavg [^{68}Ga]Ga-DOTA.SA.FAPi PET/CT (mean ± SD, range)	SULavg [^{18}F]F-FDG PET/CT (mean ± SD, range)	*P* value
Breast	6.5 ± 3.3 (3.3–12.5)	6.2 ± 1.6 (1.2–16.9)	0.921	4.9 ± 2.5 (2.2–9)	4.7 ± 2 (1–12.7)	0.911
Lung	5.8 ± 2.4 (1.2–9.6)	7.4 ± 3.8 (1.9–14.4)	0.238	4.9 ± 2.3 (2.2–9.9)	5.3 ± 3 (0.9–10.9)	0.313
Head and neck	15.4 ± 5.4 (8.6–21.2)	14.2 ± 6.7 (9.3–23.7)	0.680	8.3 ± 2.3 (5.4–10.9)	7.9 ± 2.9 (5.5–11.8)	0.783
Gall bladder	12.3	8.1	-	27	7.9	-
Ovary	8.9 ± 0.84 (7.9–9.6)	6.7 ± 1.5 (5.1–8.2)	0.199	6.8 ± 0.39 (6.3–7.1)	5.3 ± 1.2 (4.1–6.6)	0.108
Others	9.2 ± 2.5 (7.9–11.6)	9.9 ± 2 (4.7–12.8)	0.618	2.76 ± 2.5 (1.8–4. 6)	5.85 ± 2.8 (3.5–7.1)	0.071

SULpeak and avg, standardized uptake value corrected for lean body mass; *IQR*, interquartile range

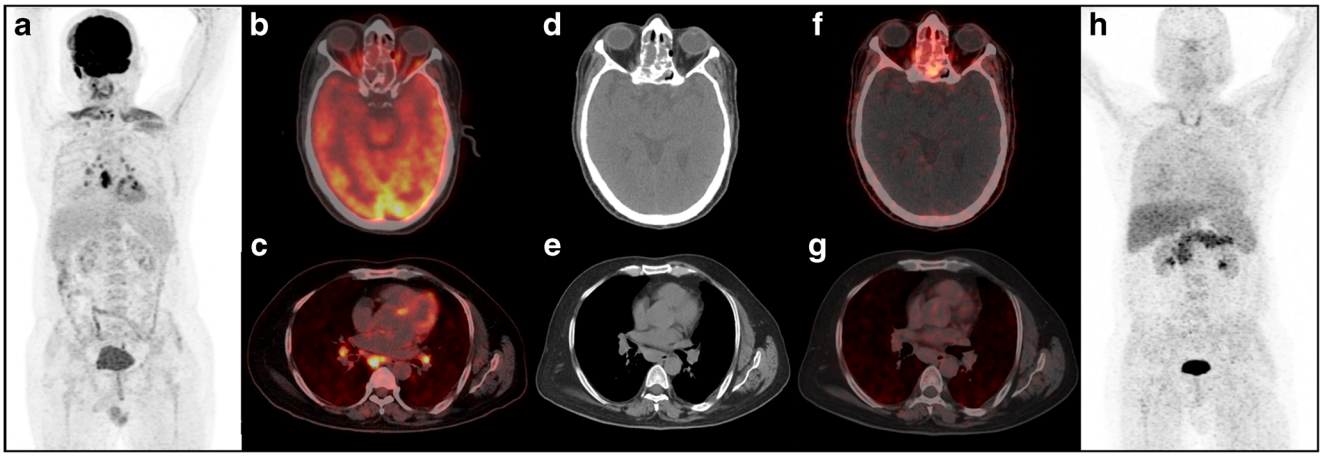

Fig. 6 In a 48-year-old man with olfactory neuroblastoma involving sphenoid fossa and ethmoidal air cells, [^{18}F]F-FDG PET/CT (**a** maximum intensity projection, **b**, **c** fused PET/CT images) and non-contrast computed tomography (**d**, **e**) revealed increased FDG uptake in the primary tumor involving the ethmoid air cells (**b**), sub-carinal and bilateral hilar lymph nodes. [^{68}Ga]Ga-DOTA.SA.FAPi PET/CT images (**f**, **g** fused PET/CT, H-maximum intensity projection) showing increased radiotracer uptake in the primary tumor only. FDG avid mediastinal lymph nodes do not show increased [^{68}Ga]Ga-DOTA.SA.FAPi uptake. He underwent endobronchial ultrasound-guided biopsy from the sub-carinal lymph node, which showed the only inflammatory infiltrate

compared to the [^{18}F]F-FDG PET/CT scans ($P < 0.0001$). One patient was detected with avid uptake in the stomach on both scans. The biopsy report revealed adenocarcinoma of the stomach and confirmed it as a second primary malignancy (Table 4).

Discussion

This study provides the first comprehensive assessment of the biodistribution, pharmacokinetics, and dosimetry of [^{68}Ga]Ga-DOTA.SA.FAPi and additionally performed a head-to-head comparison of uptake patterns between [^{68}Ga]Ga-DOTA.SA.FAPi and [^{18}F]F-FDG PET/CT.

Previously, FAP inhibitor like FAPI-02 and FAPI-04 has been developed, and the first results on the role of these agents were revealed by Giesel et al. [9] and Kratochwil et al. [10]. Among the two ^{68}Ga-labeled radiopharmaceuticals, though both agents are rapidly taken up in the lesions with almost complete internalization after 1 h in the tumor cells and have shown similar effective doses, Giesel et al. [9] found [^{68}Ga]Ga-FAPI-04 to exhibit a longer residence time of the

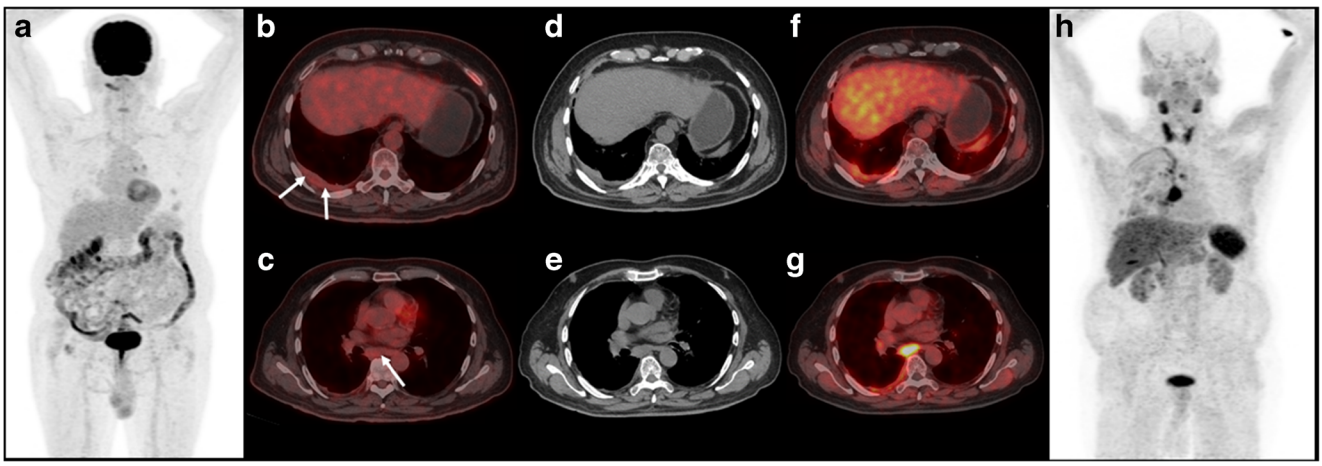

Fig. 7 72-year-old man with a known case of type 2 diabetes mellitus and a diagnosed case of mesothelioma of right pleura underwent both [^{18}F]F-FDG PET/CT and [^{68}Ga]Ga-DOTA.SA.FAPi PET/CT for staging. [^{18}F]F-FDG PET/CT images (**a**, **b**, **c**) and corresponding non-contrast CT images (**d**, **e**) showing only mild FDG uptake in the irregular right pleural thickening and sub-carinal lymph node (arrows). [^{68}Ga]Ga-DOTA.SA.FAPi PET/CT images (**f**, **g** fused PET/CT, **h** maximum intensity projection) showing intense [^{68}Ga]Ga-DOTA.SA.FAPi uptake in the right pleural thickening and sub-carinal lymph node. Physiological uptake of [^{68}Ga]Ga-DOTA.SA.FAPi is seen in liver, spleen, pancreas, thyroid glands, salivary glands, lacrimal glands, kidney, and urinary bladder, and also noted mild diffuse [^{68}Ga]Ga-DOTA.SA.FAPi uptake in the visualized skeletal muscles. Biopsy from the sub-carinal lymph node revealed metastases from mesothelioma

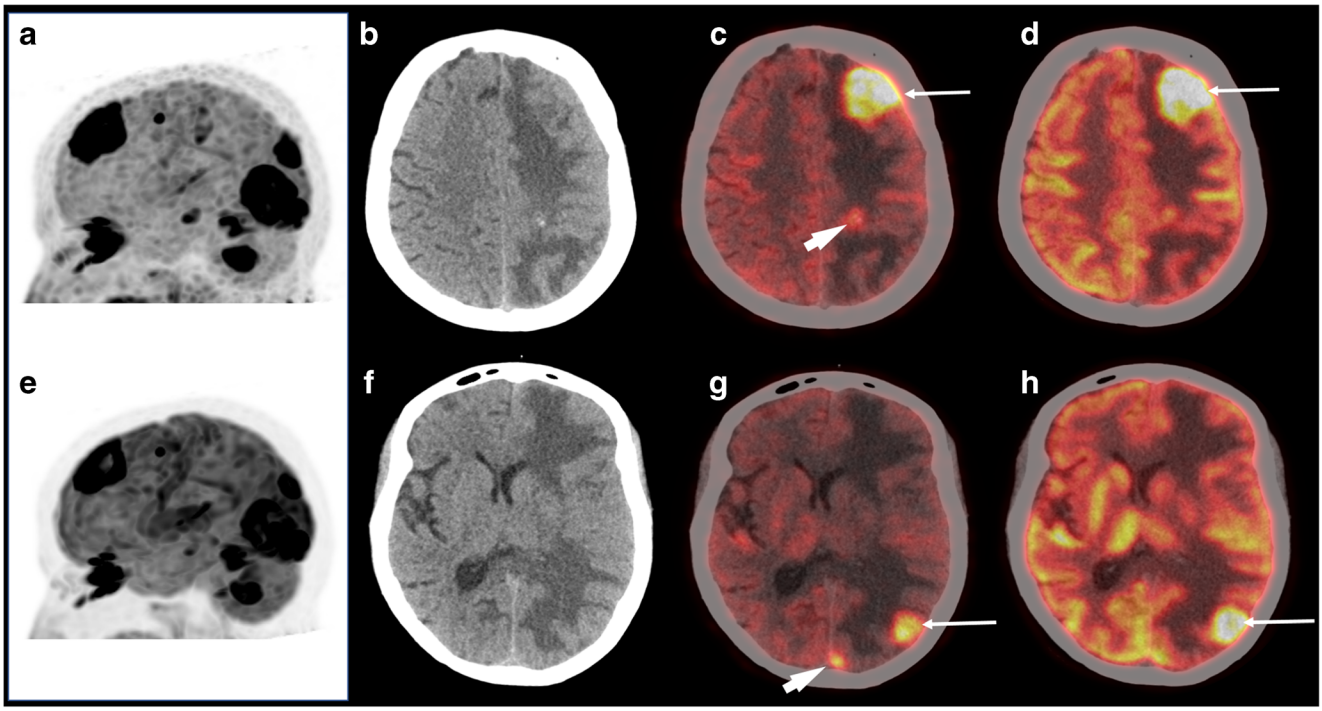

Fig. 8 A 66-year-old woman with a known case of carcinoma breast with brain metastases underwent both [^{68}Ga]Ga-DOTA.SA.FAPi PET/CT (**a**, **c**, **g**) and [^{18}F]F-FDG PET/CT (**e**, **d**, **h**) for restaging. Maximum intensity projection images (**a**, **e**) showing multiple foci of intense tracer uptake in both PET/CT. Axial sections of non-contrast computed tomography images revealed ill-defined iso dense lesions in the left frontal, parietal, and occipital lobes with perilesional edema (**b**, **f**). Corresponding fused PET/CT images of both PET/CT scans showing increased FDG uptake in these lesions (**c**, **d**, **g**, **h** arrows). [^{68}Ga]Ga-DOTA.SA.FAPi PET/CT images also revealed small occult lesions in the left parietal and left occipital lobe (**c**, **g** arrowhead)

radiotracer compared to FAPI-02 in the lesions attributed by the structural modification in the proline ring (4,4-difluoroproline) of FAPI-04.

To make an ideal radio-ligand, particularly for theranostic use, one has to match the biological half-life of a pharmaceutical agent with that of the physical half-life of radionuclide in order to deliver maximum radiation absorbed dose to the desired targets. Further research has been carried out by Loktev et al. [12] who explored 15 novel linker variations in the UAMC1110-based FAP inhibitor labeled with gallium-68 and lutetium-177 in HT-1080-FAP tumor-bearing mice and compared them with FAPi-04 molecule. Among the FAPI compounds developed by the Heidelberg group, FAPI-21 and FAPI-46 exhibited the highest tumor-to-background ratios. Moon et al. [13] attempted to focus on better tumor retention and introduced a squaric acid (SA) motif into the linker of the FAP inhibitor UAMC1110-based structures, yielding DATA^{5m}.SA.FAPi and DOTA.SA.FAPi products. The groups at Antwerp [8] and Mainz [13] confirmed extraordinarily high binding affinities in FAP binding assays in vitro at the nanomolar level combined with more than 1000-fold selectivity against other proteases. They conducted a radiochemical evaluation with gallium-68 and lutetium-177 and confirmed high tumor uptake and good tumor-to-background ratios in their in vivo microPET and ex vivo biodistribution studies on xenograft models. Following the above results, we consequently initiated a clinical study by labeling the FAP inhibitor tracer molecule DOTA.SA.FAPi with gallium-68. The next logical step was to test the new molecule, in a large number of cancer patients, its suitability as a theranostic vector.

Uptake

Similar to the ex vivo results of Moon et al. [13], we observed rapid uptake of [^{68}Ga] Ga-DOTA.SA.FAPi in all the organs, including the malignant lesions, within 10 min of intravenous injection. We observed that the maximum TBR in the lesions increased over time up to 3-h time-point scan, reflecting the stable uptake in the lesions with imperceptible washout and rapid clearance of radiotracer from the non-target organs and, hence, reducing the radiation burden to the normal organs. A rapid accumulation of activity was observed in the urinary bladder with twice the increase in the activity at 60 min p.i., indicating rapid renal clearance which is reconfirmed with the minimal absorbed dose estimate to the kidneys (2.62E-02 mSv/MBq). Although TBR improved over time, there were no additional benefits in delayed imaging; thus, diagnostic level scans could be acquired as early as 10 min p.i.

Kinetics

Well, in line with previous studies on various FAPI tracers [9, 11], a similar pattern of radiotracer kinetics has been obtained with [^{68}Ga] Ga-DOTA.SA.FAPi wherein the radiotracer washout from the non-target organs is rapid, thus, giving superior image contrast.

Blood clearances Meyer et al. [11] using [^{68}Ga]Ga-FAPI-46 showed a 50% decrease in the activity from the blood at 1 h p.i.; similarly, we observed a 40% decrease of [^{68}Ga]Ga-DOTA.SA.FAPi at 60 min p.i. from the baseline scan, and both studies observed an exponential drop in the %IA at 3 h.

Though the pancreas received the highest radiation absorbed dose, the %IA sharply dropped from 1.4 to 0.5% (60% drop) at 1 h p.i. and further reduced to 0.1% (93% decrease) at 3 h of p.i. These findings clearly indicate that the accelerated washout from the critical organ reduces the radiation burden on the pancreas. These imaging results are encouraging from the point of view of exploring ^{177}Lu/^{90}Y/^{225}Ac-labeled DOTA.SA-FAP inhibitor for therapy perspective.

Even though there were variations in the kidney absorbed doses when compared to other studies, the findings remained consistent that a similar %IA from the kidneys was excreted at 3 h p.i. We observed a 45% of the activity in the kidneys to clear at 1 h and an 80% washout by 3 h p.i. When comparing our results to that of Meyer et al. [11] in FAPI-46, it must be pointed out that though the authors observed a larger component of radiotracer (70%) washout at the initial 1 h; however, by 3 h similar to our report, they observed up to 80% decline in the %IA.

In our study, the SUV kinetics of the lesions suggested a rapid uptake, greater percentage of retention in the tumors/lesions compared to the normal organs. Meyer et al. [11] observed a 14% decrease in the SUVavg uptake in the tumor at 60 min p.i. Unlike Meyer et al., we sub-categorized SUV kinetics according to various cancer involvement sites and compared the 0.16 h and the 3 h SULpeak and avg. values. Our findings revealed the percentage decrease in the mean SUL values ranged between 5.4 and 44.3%, with the maximum difference observed in the skeletal metastases.

Giesel et al. [9] observed a 75% and 25% decline in the tumor uptake from 1 to 3 h with FAPI-02 and FAPI-04 compounds, respectively. The discrepancies pointed out the evolution of the FAPI molecules to improve tumor retention. Compared to the available studies on the SUV kinetics in tumor lesion, but similar to FAPI-46, [^{68}Ga]Ga-DOTA.SA.FAPi showed a superior tumor retention time. The difference in the retention time is no doubt due to the modification in the quinoline-based structures.

One of the significant findings that emerged from this study was that in patients with extensive tumor uptake, lesser radiotracer was available for uptake in the background organs (Fig. 2), while patients with lessor tumor burden showed higher background tracer uptake that is quite logical (Figs. 6 and 7).

Doses

The effective dose equivalent and effective dose from [^{68}Ga]Ga-DOTA.SA.FAPi were 1.64E-02 and 1.1E-02 mSv/MBq, respectively, and well in line with that of [^{68}Ga]Ga-labeled FAPI-02 and FAPI-04 and FAPI-46 radiopharmaceuticals [9] (Supplementary Table 2).

The pancreas is the critical organ that received the highest radiation absorbed dose. It is because the highest uptake was observed in the pancreas of [^{68}Ga]Ga-DOTA.SA.FAPi scan at 0.16 h p.i. Busek et al. [19] conducted an enzymatic assay in adult pancreatic tissue and demonstrated homologous proteases FAP in the islets of Langerhans. The pancreatic islets constitute 1–2% of the pancreas volume; however, they receive 10–15% of its blood flow. This expression could probably relate to the avid uptake of [^{68}Ga]Ga-DOTA.SA.FAPi in the pancreas.

In concordance with the biodistribution of [^{68}Ga]Ga-FAPI-21 [12], we observed a high expression of DOTA.SA.FAPi in the salivary thyroid glands and, to a less extent, in the lacrimal glands and in the oral mucosa. The synthetic modifications in the FAPi molecule could attribute to its variability in the biodistribution pattern.

FAPi vs. FDG

In our study, while the highest uptake of [^{68}Ga]Ga-DOTA-SA-FAPi (SUL > 10) was found in head and neck cancers followed by gall bladder carcinoma, an uptake > 5 was observed in all other cancers. Though there was a similarity in the visual analysis between FAPi-02, FAPI-04, and DOTA.SA.FAPi in various cancers, Kratochwil et al. [10] reported the highest intensity of FAPI-04 uptake in lung cancer followed by breast, esophageal cancer, cholangiocellular carcinoma, and sarcoma. On the other hand, Chen et al. [20] observed the highest uptake of [^{68}Ga]Ga-DOTA-FAPI-04 in pancreatic cancer, liver cancer (including cholangiocarcinoma and hepatocellular carcinoma), sarcoma, esophageal cancer, and gastric cancer.

While, in our study, the average SULpeak uptake for patients with breast cancer ranged between 3.3 and 12.5 on [68Ga]Ga-DOTA.SA.FAPi, Kratochwil et al. [10] observed an average SUVmax of > 12 in breast cancer patients, but, in agreement, both the tracers demonstrated a high agreement with the [^{18}F]F-FDG in the detection of lesions. The variation in the histopathology of breast cancer, the method of SUV measurements adopted in the study, and the tissue changes due to the effects of previous treatment may probably cause the variation of the SUV value. Hence, uptake in terms of

SUV and residence time depends on individual tumors and on individual expression of a given disease. It is also an important aspect that the biological probe should match the radionuclide physical half-life for therapy to give the best result; thus, SUV is not the only criterion on which theranostic agent is chosen. In this regard, our group has reported proof-of-principle work on [^{68}Ga]Ga-DOTA.SA.FAPi PET/CT-guided [^{177}Lu]Lu-DOTA.SA.FAPi radionuclide therapy in an end-stage breast cancer patient, which has proved the potential to open new applications for cancer therapeutics [14]. Garin and colleagues [5] best characterized FAP expression in the breast tissue where the authors demonstrated FAP expression exclusively in the stroma of the breast cancer and, interestingly, neither the malignant epithelial cells nor in the stroma of the adjacent normal breast tissue expressed FAPs.

We analyzed 13 patients with NSCLC, and the number of lesions correlated well between both tracers, except in one patient where [^{68}Ga]Ga-DOTA.SA.FAPi was not expressed in the lymph nodes. Liao et al. [21] illustrated the expression of FAP in paraffin-embedded primary NSCLC specimens of 50 NSCLC. The results provided important insights regarding the high expression of FAP as a prognostic indicator of poor survival.

Both [^{68}Ga]Ga-DOTA.SA.FAPi PET/CT and [^{18}F]F-FDG PET/CT demonstrated equivalent and high SUL uptake values in the primary site of head and neck cancers. In this context, Wang et al. [22] have shown a selective expression of FAP in oral squamous cell carcinoma patients. However, we studied only a small patient cohort with oral SCC; hence, it is too early to comment on the role of [^{68}Ga]Ga-DOTA.SA.FAPi in the above histological category of patients.

Among our series of patients, in two patients, the [^{68}Ga]Ga-DOTA.SA.FAPi identified additional lesions in the brain that could not be detected on [^{18}F]F-FDG PET/CT. The distinctly lower brain parenchyma uptake of [^{68}Ga]Ga-DOTA.SA.FAPi scan makes it an ideal tracer to detect brain metastases, and needless to mention is far superior to [^{18}F]F-FDG PET/CT in detecting brain tumors.

Krukenberg tumors were detected in two patients who had primary breast carcinomas. A significantly avid expression was observed with [^{68}Ga]Ga-DOTA.SA.FAPi, in contrast to the [^{18}F]F-FDG uptake. While no data regarding the expression of FAP has been recorded in literature until now, studies have shown stromal positivity in 92% of ovarian cancer tissues with extremely rare FAP expression in malignant cells [23].

Interestingly, Chen et al. [20] studied 12 different cancers in 75 patients and reported a superior detection rate of [^{68}Ga]Ga-FAPI-04 PET/CT over conventional [^{18}F]F-FDG PET/CT (98.2% vs. 82.1%) in the diagnosis of various primary tumors; however, we could not show that great difference in our head-to-head comparative study. The underlying reason for this difference is that unlike Chen et al., who studied various cancers where FDG plays a limited role, in our study, a significant percentage of patients constituted breast cancer and lung cancers where FDG is avidly expressed. The results may vary in the wider population in different clinical settings. Our results were in close agreement with the study of Kratochwil et al. [10]. Further studies on head-to-head comparison with various FAP inhibitor tracers in the same patients will need to be carried out in order to examine the ideal molecule for FAPi imaging. Accurate characterization of each type of cancer and its association with FAP expression should be studied to fully understand the implications of [^{68}Ga]Ga-FAPI PET/CT in oncologic imaging. Follow-up studies with interim [^{68}Ga]Ga-DOTA.SA.FAPi PET/CT scans could help our understanding of the role of FAPi as a prognostic indicator of treatment response and survival.

There is no one-stop-shop in oncology; it is envisaged that in the future, both FDG- and FAPI-based tumor imaging shall complement each other to cover a greater number of cancers under its banner and minimize the false-positive and false-negative findings.

Limitations

This study is accompanied by certain limitations. The sample size of the patients with different kinds of histopathology was small. This investigation must be conducted in a large population of patients to study the variability of FAPi expression and its retention in different cancers.

Conclusions

This is the first clinical study on the biodistribution and pharmacokinetics of [^{68}Ga]Ga-DOTA.SA.FAPi and demonstrates a high target-to-background ratio in various types of cancers. The mean absorbed dose to various organs and the mean effective dose from 185 MBq of [^{68}Ga]Ga-DOTA.SA.FAPi was approximately 2 mSv, which was within the safe admissible limits. [^{68}Ga]Ga-DOTA.SA.FAPi PET/CT imaging can be conducted as early as 10 min post-injection of the radiotracer. The diagnostic accuracy of [^{68}Ga]Ga-DOTA.SA.FAPi PET/CT closely matched to the standard-of-care imaging [^{18}F]F-FDG-PET/CT. The findings clearly indicate the selective expression of [^{68}Ga]Ga-DOTA.SA.FAPi in various cancers makes a contribution to the current literature on FAP inhibitor molecular imaging. It provides an additional role of FAPi in the field of theranostics.

In future, large-scale multicenter studies with a homogenous patient population in different cancer types should be tested with a head-to-head comparison with the FAPi-02, 04, DOTA.SA.FAPi, and FAPi-46 molecules to best comment on the superiority of the tracers.

Supplementary Information The online version contains supplementary material available at https://doi.org/10.1007/s00259-020-05132-y.

Data availability The data and material are available.

Compliance with ethical standards

Conflict of interest The authors declare that they have no conflict of interest.

Ethical clearance Ref. No IECPG-22/2020.

Informed consent we obtained written informed consent from all the patients before commencing the investigational PET/CT Scan.

Disclaimer The current work has not been submitted for review or is not under acceptance for publication in any journal.

References

1. Warburg O, Wind F, Negelein E. The metabolism of tumors in the body. J Gen Physiol. 1927;8:519–30.
2. Mankoff DA, Eary JF, Link JM, Muzi M, Rajendran JG, Spence AM, et al. Tumor-specific positron emission tomography imaging in patients: [18F] fluorodeoxyglucose and beyond. Clin Cancer Res. 2007;13:3460–9.
3. Chang JM, Lee HJ, Goo JM, Lee HY, Lee JJ, Chung JK, et al. False positive and false negative FDG-PET scans in various thoracic diseases. Korean J Radiol. 2006;7:57–69.
4. Davidson B, Trope CG, Reich R. The role of the tumor stroma in ovarian cancer. Front Oncol. 2014;4:104.
5. Garin-Chesa P, Old LJ, Rettig WJ. Cell surface glycoprotein of reactive stromal fibroblasts as a potential antibody target in human epithelial cancers. Proc Natl Acad Sci. 1990;87:7235–9.
6. Cheng DJ, Dunbrack RL, Valianou M, Rogatko A, Alpaugh RK, Weine LM. Promotion of tumor growth by murine fibroblast activation protein, a serine protease, in an animal model. Cancer Res. 2002;62:4767–72.
7. Liu R, Li H, Liu L, Yu J, Ren X. Fibroblast activation protein: a potential therapeutic target in cancer. Cancer Biol Ther. 2012;13:123–9.
8. Jansen K, Heirbaut L, Verkerk R, Cheng JD, Joossens J, Cos P, et al. Extended structure-activity relationship and pharmacokinetic investigation of (4-quinolinoyl)glycyl-2-cyanopyrrolidine inhibitors of fibroblast activation protein (FAP). J Med Chem. 2014;57:3053–74.
9. Giesel FL, Kratochwil C, Lindner T, Marschalek MM, Loktev A, Lehnert W, et al. 68Ga-FAPI PET/CT: biodistribution and preliminary dosimetry estimate of 2 DOTA-containing FAP-targeting agents in patients with various cancers. J Nucl Med. 2019;60:386–92.
10. Kratochwil C, Flechsig P, Lindner T, Abderrahim L, Altmann A, Mier W, et al. 68Ga-FAPI PET/CT: tracer uptake in 28 different kinds of cancer. J Nucl Med. 2019;60:801–5.
11. Meyer C, Dahlbom M, Lindner T, Vauclin S, Mona C, Slavik R, et al. Radiation dosimetry and biodistribution of 68Ga-FAPI-46 PET imaging in cancer patients. J Nucl Med. 2020;61:1171-7.
12. Loktev A, Lindner T, Burger EM, Altmann A, Giesel F, Kratochwil C, et al. Development of fibroblast activation protein-targeted radiotracers with improved tumor retention. J Nucl Med. 2019;60:1421–9.
13. Moon ES, Elvas F, Vliegen G, Lombaerde SD, Vangestel C, Bruycker SD, et al. Targeting fibroblast activation protein (FAP): next generation PET radiotracers using squaramide coupled bifunctional DOTA and DATA 5m chelators. EJNMMI Radiopharm Chem. 2020;5:19. https://doi.org/10.1186/s41181-020-00102-z.
14. Ballal S, Yadav MP, Kramer V, Moon ES, Roesch F, Tripathi M, et al. A theranostic approach of [68Ga]Ga-DOTA.SA.FAPi PET/CT-guided [177Lu]Lu-DOTA.SA.FAPi radionuclide therapy in an end-stage breast cancer patient: new frontier in targeted radionuclide therapy. Eur J Nucl Med Mol Imaging. 2020. https://doi.org/10.1007/s00259-020-04990-w.
15. Valentin J. Basic anatomical and physiological data for use in radiological protection: reference values. A report of age- and gender-related differences in the anatomical and physiological characteristics of reference individuals. ICRP Publication 89. Ann ICRP. 2002;32:1–277.
16. Ferrer L, Kraeber-Bodere F, Bodet-Milin C, Rousseau C, Gouill SL, Wegener WA, et al. Three methods assessing redmarrow dosimetry in lymphoma patients treated with radioimmunotherapy. Cancer. 2010;116:1093–100.
17. Wahl RL, Jacene H, Kasamon Y, Lodge MA. From RECIST to PERCIST: evolving considerations for PET response criteria in solid tumors. J Nucl Med. 2009;50(Suppl 1):122–50.
18. Mandrekar JN. Measures of interrater agreement. J Thorac Oncol. 2011;6(1):6–7.
19. Busek P, Hrabal P, Fric P, Sedo A. Co-expression of the homologous proteases fibroblast activation protein and dipeptidyl peptidase-IV in the adult human Langerhans islets. Histochem Cell Biol. 2015;143:497–504.
20. Chen H, Pang Y, Wu J, Zhao L, Hao B, Wu J, et al. Comparison of [68Ga]Ga-DOTA-FAPI-04 and [18F] FDG PET/CT for the diagnosis of primary and metastatic lesions in patients with various types of cancer. Eur J Nucl Med Mol Imaging. 2020;47:1820–32.
21. Liao Y, Ni Y, He R, Liu W, Du J. Clinical implications of fibroblast activation protein-α in non-small cell lung cancer after curative resection: a new predictor for prognosis. J Cancer Res Clin Oncol. 2013;139:1523–8.
22. Wang H, Wu Q, Liu Z, Luo X, Fan Y, Liu Y, et al. Downregulation of FAP suppresses cell proliferation and metastasis through PTEN/PI3K/AKT and Ras-ERK signaling in oral squamous cell carcinoma. Cell Death Dis. 2014;5:e1155.
23. Zhang Y, Tang H, Cai J, Zhang T, Guo J, Feng D, et al. Ovarian cancer-associated fibroblasts contribute to epithelial ovarian carcinoma metastasis by promoting angiogenesis, lymphangiogenesis and tumor cell invasion. Cancer Lett. 2011;303:47–55.